

Microwave-Assisted Synthesis and Evaluation of the Optoelectronic Properties of Metallated *Meso*-Tetraphenylporphyrin Complex

Rosalio Velarde-Barraza, Edgar A. Reynoso-Soto, Ignacio A. Rivero*

Tecnológico Nacional de México/Instituto Tecnológico de Tijuana, Centro de Graduados e Investigación en Química, Blvd. Alberto Limón Padilla S/N 22510 Tijuana, B. C., México.

*Corresponding author: Ignacio A. Rivero, email: irivero@tectijuana.mx

Received October 20th, 2023; Accepted April 11th, 2024.

DOI: <http://dx.doi.org/10.29356/jmcs.v69i2.2156>

Abstract. In the present work, we report the synthesis of 5,10,15,20-tetraphenylporphyrin and the formation of its complex after insertion of a metal center with Mg^{+2} , Co^{+2} , Ni^{+2} , Cu^{+2} , or Zn^{+2} . 1H -NMR determined the insertion with signal suppression of the internal hydrogens present in the free base of the porphyrin macrocycle. UV-vis characterization shows the absorption bands of the porphyrinic systems at 418 nm and 510-650 nm. The insertion of the metal centers generates bathochromic and hypsochromic changes in the Mg^{+2} and Co^{+2} insertions, respectively, as well as changes in the molar absorptivity coefficients. The fluorescence quantum yields for some elements were almost wholly reduced, mainly for the Co^{+2} and Cu^{+2} insertions, while Mg^{+2} presented a high fluorescence quantum yield. These observations agree with the results obtained by DFT and TD-DFT, in which the oscillator strength values for the Mg^{+2} chelate are higher even than those for the 5,10,15,20-tetraphenylporphyrin free base. The electrochemical properties of the cyclic voltammetry study show four reversible oxidation and reduction peaks for the free base 5,10,15,20-tetraphenylporphyrin. Generally, the metallated *meso*-tetraphenylporphyrins show three reversible peaks of oxidation and reduction. All synthesized analogs' first oxidation potentials ranged from 0.346 to 0.804 V vs. SCE. In comparison, the first reduction potential ranged from -1.032 to -1.602 V vs. SCE, which gives great interest in their implementation as optoelectronic materials and even as materials for the elaboration of electrochemical sensors.

Keywords: Porphyrins; metallated porphyrin; DFT; cyclic voltammetry.

Resumen. En el presente trabajo reportamos la síntesis de 5,10,15,20-tetrafenilporfirina y formación de sus complejos tras la inserción de un centro metálico con Mg^{+2} , Co^{+2} , Ni^{+2} , Cu^{+2} o Zn^{+2} . La inserción fue determinada por 1H -NMR con la supresión de la señal de los hidrógenos internos presentes en la base libre del macrociclo porfirínico. La caracterización por UV-vis muestra las bandas de absorción de los sistemas porfirínicos a 418 nm y 510-650 nm. La inserción de los centros metálicos genera cambios batocrómicos e hipsocrómico en las inserciones de Mg^{+2} y Co^{+2} , respectivamente, al igual que cambios en los coeficientes de absorptividad molar¹. Los rendimientos cuánticos de fluorescencia para algunos elementos fueron reducidos casi en su totalidad, principalmente para las inserciones de Co^{+2} y Cu^{+2} , mientras que Mg^{+2} presentó un rendimiento cuántico de fluorescencia alto. Estas observaciones son concordantes con los resultados obtenidos mediante DFT y TD-DFT, en los cuales los valores de la fuerza del oscilador para el quelato de Mg^{+2} es mayor incluso que para la base libre 5,10,15,20-tetrafenilporfirina. El estudio de las propiedades electroquímicas mediante voltamperometría cíclica muestra cuatro picos reversibles de oxidación y reducción para la base libre 5, 10, 15, 20-tetrafenilporfirina, mientras de manera general para las metaloporfirinas muestran tres picos reversibles de oxidación y reducción. El primer potencial de oxidación para todos los análogos sintetizados se encontraron entre 0.346 a 0.804 V vs. SCE, mientras que el primer potencial de reducción osciló entre -1.032 a -1.602 V

vs. SCE, lo que otorga gran interés en su implementación como materiales optoelectrónicos e incluso como materiales para la elaboración de sensores electroquímicos.

Palabras clave: Porphirina; porfirina metálica; DFT; voltamperometría cíclica.

Introduction

Porphyric structures are a group of organic compounds that are widespread in nature and, from a molecular point of view, have a unique chemical structure. The base or central ring of any porphyrin consists of a cyclic tetrapyrrole group (four pyrrole rings), which, when conjugated, become colorful chromophores and can coordinate various metals through the nitrogen atoms of the pyrrole rings. [1] These structures belong to the prosthetic groups, some responsible for the specific binding of different groups to proteins. [2] In porphyrins, the external substituents determine the molecule's electronic properties, while the metal coordinated center is responsible for the binding of diatomic gases, catalysis, and redox chemistry. [3,4] Porphyric structures exhibit rich chemical properties and unique photophysical properties; therefore, they are attractive for design and search for new analogs with tunable photophysical and electronic properties targeted to the research field. [5–8]

The synthesis of the porphyric macrocycle can be carried out in different ways and using different materials; however, even at present, the yields of the material obtained represent a limitation. [6,9,10] However, this is different in the case of metalation or insertion of the metal centers into the macrocyclic structure. The most effective methodology is using microwaves as a thermal energy source. This is because it provides a set of unattainable reaction conditions by conventional heating. This technique leads to a remarkable decrease in reaction times and increased reaction yields. [11–13] This has generated the emergence of several porphyric metal complexes as molecular catalysts for the electrochemically triggered hydrogen evolution reaction, [14] in the evaluation of antimicrobial activities, [15] in the detection of analytes such as dopamine and uric acid, [16] in the electrocatalytic reduction of CO₂, [17] and even as sensitizers for dye-sensitized solar cells (DSSC).¹⁸ Based on the above, we performed the synthesis of the meso-tetraphenylporphyrin and the insertion of different metal centers under microwave heating to evaluate their optoelectronic properties. The chosen transition metals are widely used in electrochemical studies, and the alkaline-earth element Mg⁺² was included to evaluate its acid-base properties on the above mentioned properties. The ultraviolet-visible spectroscopy and fluorescence emission studies denoted the changes in their optical properties due to the metal centers. In contrast, the theoretical studies by density functional theory (DFT) helped in the determination of the energy levels of the most allowed transitions, which were compared with the experimental evaluations by cyclic voltammetry in order to determine the viability of the different metallic elements for their usefulness in different research fields for many applications such as optoelectronics, sensing, and bioimaging.

Materials and methods

General procedure

All solvents and reagents were purchased commercially (Sigma-Aldrich, Saint Louis, USA) and used without further purification. The isolation and purification of the products of interest were performed first by thin layer chromatography (TLC) on silica gel F₂₅₄ plates and then by column chromatography using Silica gel 60 (230-400 mesh). The ¹H and ¹³C NMR spectra at 200 and 50 MHz, respectively, were obtained using a Varian Mercury 200 MHz spectrometer. All spectra were obtained using CDCl₃ as solvent and TMS as internal standard. Mass spectra were obtained by direct insertion in an Agilent Technologies 5975C mass spectrometer at 70 eV SL version coupled to an Agilent HPLC (Mod 1100). Absorption studies were obtained on a Varian Cary 50 UV-vis spectrophotometer.

Preparation of *meso*-tetraphenylporphyrin free base (3)

Following the method of Adler, [19] 1.5 mmol of pyrrole (104 μL), 1.5 mmol of benzaldehyde (153 μL), and 1.5 mmol of trifluoroacetic acid (115.8 μL) were added to a 250 mL flask, and dissolved in 150 mL of dry dichloromethane under argon atmosphere with room temperature and constant stirring for 2 hours. Upon completion, 1.128 mmol of 2,3-dichloro-5,6-dichloro-5,6-dicyano-1,4-benzoquinone (DDQ) (256 mg) was added and allowed to react at reflux for 1 h at 40° C under constant stirring. Subsequently, the solvent was removed by vacuum, washed with sodium thiosulfate, and finally, the crude product was purified by column chromatography using dichloromethane as eluent to obtain a purple powder (100 mg, 43 %). UV-Vis (CH_2Cl_2) λ / nm 418; 517; 550; 593, 647; FT-IR (attenuated total reflectance (ATR), neat) $\tilde{\nu}$ / cm^{-1} 698, 725, 798, 964, 980, 1072, 1178, 1348, 1441, 1595, 3020, 3053, 3315; ^1H NMR (CDCl_3 , 200 MHz, 25 °C) δ ppm: δ 8.89 (s, 8H), δ 8.27 (dd, $J=7.6, 1.7$ Hz, 8H), δ 7.78 (m, 12H), δ -2.68 (s, 2H). ^{13}C NMR (CDCl_3 , 50 MHz, 25 °C) δ 142.2, 134.5, 127.7, 126.7, 120.2. ESI-MS (m/z): $[\text{C}_{45}\text{H}_{30}\text{N}_4]^+$ [calculated for $\text{M}+\text{H}^+$]: 615.0, [found]: 615.2.

Microwave-assisted synthesis of metallated *meso*-tetraarylporphyrins

Metallated *meso*-tetraphenylporphyrins were prepared as reported by Önal *et al.* with slight modifications. [20] A mixture of 0.083 mmol of porphyrin and 0.406 mmol of metal acetate was dissolved in 5 mL of dimethylformamide (DMF). It was subjected to microwave irradiation at a temperature of 160 °C for 5 min and 200 Watts. After reaction time was accomplished, the porphyrins precipitated with CH_3OH . The crude solid was filtered, washed three times with CH_3OH , and dried to obtain the corresponding metallated *meso*-tetraphenylporphyrin.

Magnesium 5,10,15,20-tetraphenylporphyrin (4a). Yield: 95 %. UV-Vis (CH_2Cl_2) λ / nm 425; 568; FT-IR (attenuated total reflectance (ATR), neat) $\tilde{\nu}$ / cm^{-1} 753, 798, 994, 1007, 1064, 1174, 1200, 1331, 1439, 1480, 1593, 3564, 3647; ^1H NMR (CDCl_3 , 200 MHz, 25 °C): δ 8.82 (s, 8H), δ 8.20 (m, 8H), δ 7.71 (m, 12H); ^{13}C NMR (CDCl_3 , 50 MHz, 25 °C) δ 150.0, 144.0, 134.8, 131.8, 127.1, 126.4, 121.6.

Cobalt 5,10,15,20-tetraphenylporphyrin (4b). (*Paramagnetic compound*) Yield: 80 %. UV-Vis (CH_2Cl_2) λ / nm 410;537; FT-IR (attenuated total reflectance (ATR), neat) $\tilde{\nu}$ / cm^{-1} 748, 794, 1002, 1067, 1205, 1348, 1441, 1540, 1598, 1668, 3048.

Nickel 5,10,15,20-tetraphenylporphyrin (4c). Yield: 90 %. UV-Vis (CH_2Cl_2) λ / nm 418; 527; FT-IR (attenuated total reflectance (ATR), neat) $\tilde{\nu}$ / cm^{-1} 696, 708, 742, 793, 1007, 1072, 1350, 1439, 1599, 2922, 3022, 3052; ^1H NMR (CDCl_3 , 200 MHz, 25 °C): δ 8.73 (s, 8H), δ 8.00 (m, 8H), δ 7.67 (m, 12H); ^{13}C NMR (CDCl_3 , 50 MHz, 25 °C) δ 142.7, 142.2, 134.6, 133.7, 132.2, 127.7, 126.9, 126.7.

Copper 5,10,15,20-tetraphenylporphyrin (4d). (*Paramagnetic compound*) Yield: 92 %. UV-Vis (CH_2Cl_2) λ / nm 415; 538; FT-IR (attenuated total reflectance (ATR), neat) $\tilde{\nu}$ / cm^{-1} 696, 710, 741, 793, 1005, 1070, 1344, 1439, 1597, 3022, 3051.

Zinc 5,10,15,20-tetraphenylporphyrin (4e). Yield: 90 %. UV-Vis (CH_2Cl_2) λ / nm 419; 548; FT-IR (attenuated total reflectance (ATR), neat) $\tilde{\nu}$ / cm^{-1} 702, 717, 750, 798, 1001, 1066, 1174, 1338, 1441, 1595, 2852, 2924; ^1H NMR (CDCl_3 , 200 MHz, 25 °C): δ 8.99 (s, 8H), δ 8.26 (dd, 8H), δ 7.78 (m, 12H); ^{13}C NMR (CDCl_3 , 50 MHz, 25 °C) δ 150.3, 143.0, 134.6, 132.1, 127.6, 126.7, 121.3.

UV-Vis studies

UV-Vis data were recorded on samples in dichloromethane (DCM) solution at 1×10^{-6} mol L^{-1} . The absorbance A was measured at 200 to 800 nm wavelengths with a Varian Cary 50 scan spectrophotometer. To the DCM solution, 1 molar equivalent of the corresponding porphyrin was added until the absorbance reached 1 a.u., and linear regression of maximum absorbance data was carried out to obtain molar absorptivity ($\epsilon_{\text{max}} / \text{M}^{-1} \text{cm}^{-1}$). Zinc phthalocyanine was used as the standard sample under the same conditions.

Computational study

The Gaussian 09 program performs theoretical calculations using density functional theory (DFT). The ground state geometry of *meso*-tetraphenylporphyrin free base and each metallated *meso*-tetraphenylporphyrin analog was optimized with the B3PW91 exchange-correlation function, and a set of 6-31G basis calculations was applied. Vibrational frequency calculations were performed simultaneously to validate that the obtained structures were at the minimum potential energy surface, and finally, time-dependent density functional theory (TD-DFT) analysis was performed.

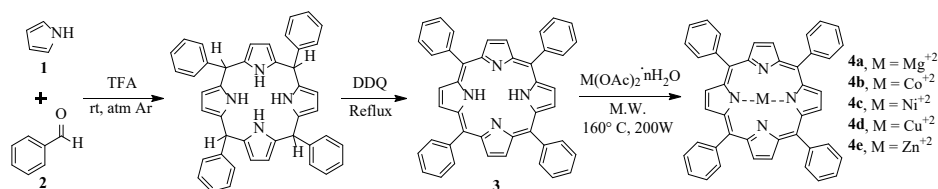
Cyclic voltammetry

Cyclic voltammetry measurements were carried out in a potentiostat/galvanostat Biologic model VMP300. Three electrode arrangement was employed with a platinum wire as a counter electrode, Ag/AgNO₃ as a reference electrode, and vitreous carbon as the working electrode. The experiments were made in an electrolyte solution of tetrabutylammonium hexafluorophosphate at 0.1 mol L⁻¹ with ferrocene/ferrocenium (Fc/Fc⁺) redox par at 2 μmol L⁻¹ and the porphyrin sample at 1 μM and bubbled with N₂.

Results

Synthesis of *meso*-tetraphenylporphyrins and metallated analogs

The synthesis of the *meso*-tetraphenylporphyrin analog (**3**) was performed using the classical pyrrole condensation reaction reported previously (Scheme 1). [19,21,22] Performing the first step of the reaction under an inert atmosphere of argon is a crucial point for the synthesis of our product of interest because it helps to avoid as much as possible the oxidation of the aldehyde and helps to increase the formation of the macrocyclic intermediate porphyrinogen, which later, in a second step is oxidized for the generation of the conjugation of the double bonds in the ring. The purification process on silica gel gave us a dark purple product with a yield of 43 %. In FT-IR spectra, we observed the characteristic signals of the conjugated system: at 698 and 798 cm⁻¹, the aromatic C–H out-of-plane tensions: at 1348 cm⁻¹, the C–N tension: at 1556 and 1595 cm⁻¹, the C=C tensions: at 3020 and 3053 cm⁻¹, and the N–H tension: at 3315 cm⁻¹. ¹H NMR spectrum contained signals singlet at 8.89 ppm corresponding to the β-hydrogens present in the periphery of the porphyrinic ring; signals at 8.27 and 7.78 ppm corresponding to the hydrogens in the *meso* position of the ring and at –2.68 ppm we observed a singlet that integrates for the two internal hydrogens of the porphyrinic ring.



Scheme 1. Synthesis of the *meso*-tetraphenylporphyrin free base (**3**) and metallated *meso*-tetraphenylporphyrins (**4a-e**).

The third step in Scheme 1 represents the insertion of the metal center into the structure. For this purpose, metal acetates were used in excess to ensure the coordination of the metal to the porphyrin. In the first attempt, the synthesis was carried out using dichloromethane under reflux and constant stirring. [9,23] However, at the end of the reaction, there was remaining metal acetate, suggesting that the reaction did not proceed, which was confirmed by TLC. On the other hand, the use of dimethylformamide (DMF) as a reaction solvent and microwaves at 160 °C with 1 min intervals and constant stirring represented an effective way to insert each metal center into the structure. [20] This was corroborated by the absence of the N–H stretching vibration signals at 3315 cm⁻¹ in the FT-IR spectra and the absence of the ¹H NMR signal for the internal hydrogens at a shift of –2.68 ppm.

Photophysical properties

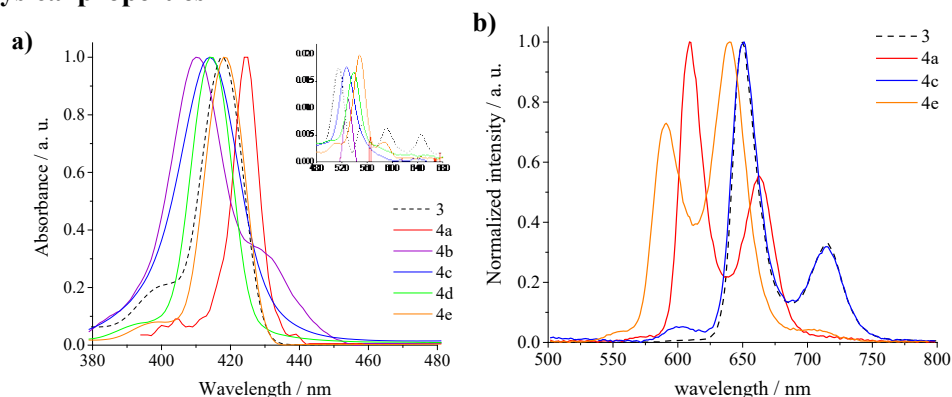


Fig. 1. UV-vis absorption spectra **(a)** and fluorescence spectra **(b)** of *meso*-tetraphenylporphyrin free base **(3)** y metallated *meso*-tetraphenylporphyrins **(4a-4e)** in DCM.

Ultraviolet-visible spectra of the free base **3** and its metallated forms **4a-4e** were recorded in DCM at room temperature and are depicted in Fig. 1**(a)**. The spectroscopic data are reported in Table 1. The spectra show the characteristic Soret bands at ~ 420 nm corresponding to $S_0 \rightarrow S_2$ transitions and the Q bands belonging to $S_0 \rightarrow S_1$ transitions between 510-650 nm. [15,24] The free base **3** presented its Soret band at 418 nm and four Q bands at 517, 550, 593, and 647 nm, while the insertion of the metal centers degenerated to the presence of a single Q band at 548 ± 20 nm. Compound **4a** presented the most significant bathochromic shift of the Soret band at 425 nm, while **4b** presented the most significant hypsochromic shift at 410 nm. The metalation of the porphyrin has a significant effect on the molar absorptivity coefficient, which is $476,392 \text{ M}^{-1} \text{ cm}^{-1}$ for the free base but is drastically reduced to $131,071 \text{ M}^{-1} \text{ cm}^{-1}$ with the insertion of Co^{+2} . In contrast, the insertion of Zn^{+2} increases the molar absorptivity coefficient.

Table 1. Absorption and emission data.

Compound	$\lambda_{\text{abs}} / \text{nm}$				$\epsilon_{\text{max}} / \text{M}^{-1} \text{ cm}^{-1}$	$\lambda_{\text{em}} / \text{nm}$	Φ_f		
Zinc Phthalocyanine	672				38,911	677	0.300		
	$\lambda_{\text{abs B}} / \text{nm}$	$\lambda_{\text{abs Q}} / \text{nm}$							
		λ_1	λ_2	λ_3	λ_4				
3	418	517	550	593	647	476,392	650; 716	0.027	
4a	425	568					314,926	609; 655	0.159
4b	410	537					131,071	654; 718	0.001
4c	414	527					276,921	650; 715	0.020
4d	415	538					376,779	650; 714	0.006
4e	419	548					533,029	595; 645	0.014

* λ_{abs} = absorption wavelength; $\lambda_{\text{abs B}}$ = Soret band absorption; $\lambda_{\text{abs Q}}$ = Q bands absorption; ϵ_{max} = molar absorption coefficient corresponding to the Soret band; nm= nanometers. *Zinc Phthalocyanine was used as a reference.

Fluorescence emission spectroscopy studies show porphyrinic compounds' characteristic dual emission bands (Fig. 1(b)). This dual emission is caused by a charge transfer produced upon excitation, which generates a locally excited state (LE, $\pi\text{-}\pi^*$) and an intramolecular charge transfer state (ICT, D^+A^-). [24,25] The free base **3** shows maximum emissions at 650 and 716 nm, while for analogs **4a** and **4e**, hypsochromic shifts up to 71 nm are observed compared to the free base. The spectrum of compound **4c** is similar to that of the free base (**3**), with only a tiny fluorescence emission shift (Fig. 1). On the other hand, the fluorescence quantum yield obtained for the free base **3** was 0.027, using zinc phthalocyanine as a reference. Analog **4a** with the Mg^{+2} metal center presented the best fluorescence emission quantum yield with a considerable increase compared to the free base **3**. This increase is considered to be due to the ability of magnesium for electronic donation compared to transition metals, where, in some cases, a quenching of the fluorescence emission is observed, especially with paramagnetic metals Co^{+2} and Cu^{+2} . [15,26,27]

Computational studies by DFT

The interest in computational studies by DFT is because they are prevalent methods for calculating systems of a specific size, especially in complexes with transition metals. This is due to the introduction of hybrids functional, the Becke three-parameter (B3) exchange functional in combination with some correlation functional (e.g., LYP and PW91) widely used for the porphyrinic system. [28–31] In addition, using a polarized basis set that considers d orbitals on non-hydrogen atoms allows us to obtain acceptable quantitative results at a low computational cost.

The optimization of the ground state geometrical structures of the free base of *meso*-tetraphenylporphyrin **3** and its metallated analogs (**4a–e**) were performed using the B3PW91/6-31G method, and continuously, carrying out a vibrational frequency analysis under the same parameters. Once these calculations were obtained, point studies used time-dependent density function theory (TD-DFT) under the same correlation functions and base set of calculations. The free porphyrin **3** presents a planar structure, which is retained even after the insertion of the Mg^{+2} , Co^{+2} , Cu^{+2} , and Zn^{+2} metal centers; these metal ions are in the plane of the porphyrin macrocycle. On the other hand, the porphyrin ring shows severe wave-like deformation after the coordination of the Ni^{+2} metal center, which is reflected in the twisting of the contour plots of its molecular orbitals (Fig. 2). [30,32] The (HOMO and LUMO) represent the sites with the highest probability in an electronic process. For most of the metallated porphyrins, the HOMO orbitals are located mainly on the four *meso*-carbons, as well as on the four-pyrrole nitrogen atoms, and in the case of the **4b** analog, there is a change in the electronic distribution after Co^{+2} insertion. In contrast, the LUMO orbitals are located on the *meso*-carbons and two opposing pyrrole carbons. These distributions are similar to some reported studies. [31,33]

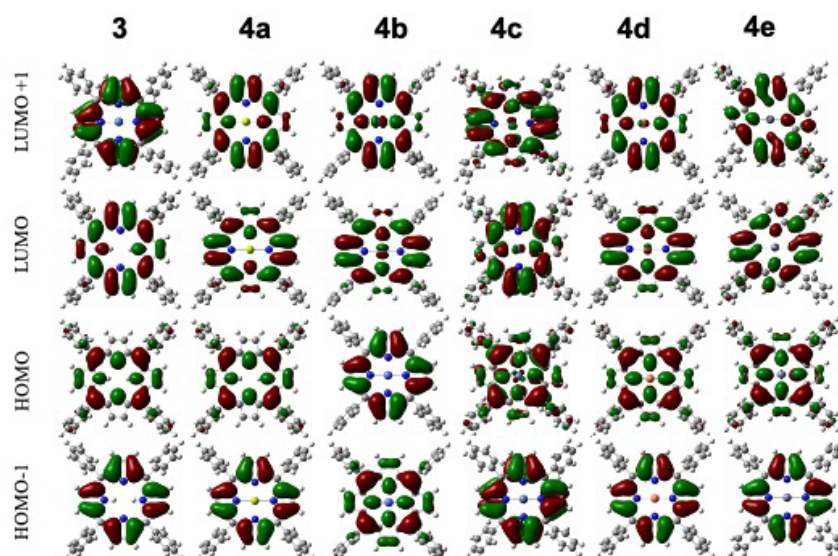


Fig. 2. The contour plots of the frontier molecular orbitals of the *meso*-tetraphenylporphyrin free base (**3**) metallated *meso*-tetraphenylporphyrin (**4a–4e**) at an isosurface value of 0.03 au.

The main molecular transitions are between two HOMO orbitals (HOMO and HOMO-1) and two LUMO orbitals (LUMO and LUMO+1). According to the Gouterman model, the Soret bands correspond mainly to transitions generated from HOMO-1 (HOMO-1→LUMO and HOMO-1→LUMO+1), while the Q bands are mainly due to transitions generated from HOMO (HOMO→LUMO and HOMO→LUMO+1), which is in agreement with the observed transitions (Table S1). [31,33,34] Overall, the levels of HOMO orbitals average -2.207 eV, while the levels of LUMO orbitals average -5.140 eV (Table 2). The energy levels of the HOMO orbitals in the metallated porphyrins present an increase of up to 0.272 eV compared to the free base **3**. In comparison, the energy levels of the LUMO orbitals of the metallated porphyrins presented a decrease of up to 0.305 eV. This implies an increase of up to 0.578 eV in the energy gap of the molecular energy levels.

In some studies, introducing donor groups that add more electrons to the porphyrinic ring system or increased electronic delocalization is critical to changing the relative energies and causing changes in the absorption and emission spectra. [24,30,31,35] In our case, the change from a transition metal to an alkali metal leads to a remarkable change in its optical properties, which are supported by the data obtained for the oscillator strength of the mostly allowed transition, being **4a** the derivative presenting a high value compared to the free base **3** as also reflected in its maximum absorption shift and its fluorescence quantum yield. Meanwhile, the oscillator strengths were low or zero for the other metal centers, especially the paramagnetic metal centers of Co⁺² and Cu⁺². These agree with their emission quantum yields, indicating a lower probability for the transition from the ground state to occur (Table 2).

Table 2. Calculated HOMO-LUMO energy levels, $\Delta E_{\text{HOMO-LUMO}}$, and oscillator strength.

	Compound					
	3	4a	4b	4c	4d	4e
LUMO	-2.3415	-2.1875	-2.0694	-2.1828	-2.2071	-2.2590
HOMO	-5.0232	-5.0273	-5.3290	-5.1214	-5.2760	-5.0631
$\Delta E_{\text{HOMO-LUMO}}$	2.6817	2.8398	3.2596	2.9386	3.0689	2.8041
Oscillator Strengths	0.6777	1.3825	0	0.0208	0	0.0586

*Energy values for HOMO-LUMO and $\Delta E_{\text{HOMO-LUMO}}$ reported in eV.

Cyclic voltammetry

For the study of the electrochemical properties of the free base **3** and its metallated complexes with Mg⁺², Co⁺², Ni⁺², Cu⁺², and Zn⁺², the studies were carried out in dichloromethane at a rate of 100 mV/s, in a measurement range comprising -2 to 1.25 V and using ferrocene (Fc/Fc⁺) as an internal standard in the analysis. The graphs obtained are shown in Fig. 3, while the oxidation and reduction potentials, as well as the energy levels of the HOMO and LUMO orbitals, are presented in Table 3. The voltammograms show four oxidation and reduction peaks for the free base **3**. The metallated porphyrins show 3 oxidation and reduction peaks, except for the analog **4b**, which presents 5 redox peaks, similar to those reported for some cobalt porphyrin analogs.³⁶ Most compounds present two bands at positive potentials corresponding to the M/M⁺ and M^{+/M²⁺} oxidation processes. The first oxidation potential for the free base **3** was 0.643 V vs. SCE, while the metallated analogs were found to be between 0.346 – 0.804 V vs. SCE, with compound **4a** having the lowest potential and **4b** the highest.

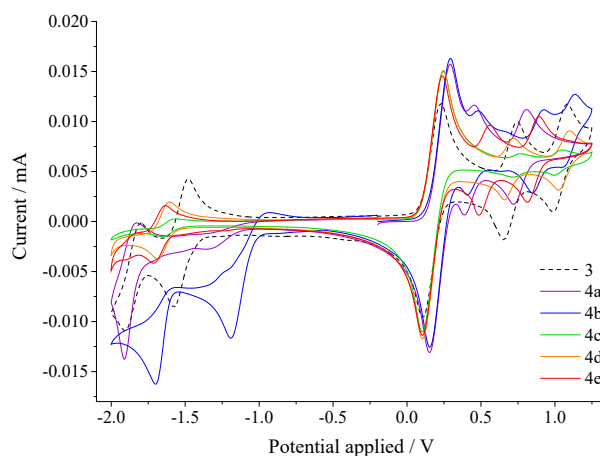


Fig. 3. Cyclic voltammetry of *meso*-tetraphenylporphyrin free base (**3**) and metallated *meso*-tetraphenylporphyrins (**4a–4e**) in DMC using Fc/Fc⁺ as reference redox couple.

Cyclic voltammetry allows estimating in a very efficient way two crucial parameters in materials aimed at the development of organic optoelectronics, the HOMO and LUMO levels, related to the ionization potential and the electronic affinity, respectively. [37] This estimation of the molecular energy levels is given by the observation of the first oxidation process at a positive potential, which is associated with the HOMO level. In contrast, the first reduction process at negative potential is associated with the LUMO level. The free base **3** presented a HOMO value of -5.743 eV, while the metallated analogs presented HOMO values from -5.446 to -5.904 eV, observing an increase in the HOMO levels for analogs **4a** and **4e**. On the other hand, the free base **3** presented a LUMO level with a value of -3.665 eV, while the metallated analogs presented LUMO levels from -3.498 to -4.068 eV, observing a decrease in the levels of analogs **4a** and **4b** (Table 3). These determinations provide us with an energy gap of 2.078 eV for the free base **3**, which, when compared to metallated porphyrins, we denoted a reduction of up to 0.577 eV for analogs **4a** and **4b**, while for analogs **4c** and **4d** an increase in the energy gap of up to 0.152 eV was observed. These determinations are based on the potential obtained for Fc/Fc⁺ of 0.4 V vs. SCE, which indicates a formal potential of -5.1 eV on the Fermi scale. [38]

Table 3. Electrochemical parameters of cyclic voltammetry.

Compound	$E_{\text{onset/Ox}}$ (V)	$E_{\text{onset/Red}}$ (V)	HOMO (eV)	LUMO (eV)	ΔE_{H-L} (V)
3	0.643	-1.435	-5.743	-3.665	2.078
4a	0.346	-1.155	-5.446	-3.945	1.501
4b	0.804	-1.032	-5.904	-4.068	1.836
4c	0.683	-1.547	-5.783	-3.553	2.230
4d	0.637	-1.577	-5.737	-3.523	2.214
4e	0.474	-1.602	-5.574	-3.498	2.076

*Sweep speed, 100 mV/s; reference electrode, Ag/AgNO₃; glassy carbon as working electrode; $E_{\text{onset/Ox}}$, oxidation potential; $E_{\text{onset/Red}}$, reduction potential.

Based on these determinations, the feasibility of its application and operation in optoelectronic devices is an evident possibility. By observing the LUMO levels of each analog, we can denote that these are above the conduction band of anodes such as TiO₂ and ZnO₂ (−4.2 and −4.3 eV, respectively), which would estimate a possible electronic transfer capacity. [2,39,40] In addition, another essential point is the levels of the HOMO orbitals of all the studied analogs, which are below the levels of some redox pairs such as iodide/triiodide (I[−]/I₃[−]) and cobalt tris(bispyridine) [Co(bpy)₃]^{2/3+} (−4.80 and −4.54 eV, respectively), which are widely used in the construction of solar cells. [41,42]

Another critical point is the wide window that these analogs present between the oxidation and reduction peaks, which range from −1.5 to 0.5 eV. This would provide the capacity to generate sensitive layers for developing electrochemical sensors to detect analytes of interest. There are reports of asymmetric *meso*-tetraphenylporphyrins used for electrochemical sensors to detect traces of histamine associated with the freshness of meat products. [43] Moreover, porphyrin analogs with metal centers can be used in areas such as electrocatalysis. There are reports of 5,10,15,20-tetrakis(4-carboxyphenyl)porphyrin complexes of cobalt as molecular catalysts supported by metal-organic frameworks that show considerable activity in hydrogen evolution reaction (HER) and oxygen reduction reaction (ORR) activity. [26,44]

Conclusions

The synthesis of *meso*-tetraphenylporphyrin by the classical pyrrole condensation reaction with an aldehyde in solution presents acceptable yields, limiting the formation of higher products or the polymerization of pyrrole caused by the acidic condition of the reaction. Additionally, the use of metal acetates in an aprotic polar solvent under microwave irradiation is a suitable way to achieve coordination of the porphyrin structure to the metals in all studied cases, as evidenced by the absence of the signal of the internal hydrogens in the porphyrin ring in FT-IR and ¹H NMR spectra. The insertion of the metal center in the porphyrin ring generates essential changes in the optical properties, such as bathochromic or hypsochromic shifts of the Soret band, changes in the molar absorptivity coefficients, and even substantial increases in the fluorescence emission upon insertion of the metal as observed in the case of Mg⁺². The DFT studies indicate that the free base and most of its metallated complexes have a planar central core with the molecular orbitals HOMO-LUMO located mainly on the four *meso*-carbons and the pyrrole nitrogen atoms. The main absorption transitions are generated primarily between the HOMO (HOMO and HOMO−1) and LUMO (LUMO and LUMO+1) orbitals. Another critical data is represented by the value of the oscillating force for the Mg⁺² analog, which presented a high value compared to the free base and corroborated the increase of the fluorescence emission for this complex.

Cyclic voltammetry studies denoted the base's oxidation-reduction processes and metallated forms. The main change was observed after the insertion of the metal center, which caused the degeneration of a redox process to the negative potential for four of the five metallated species. On the other hand, the determinations of the oxidation-reduction potentials experimental estimate of the energetic levels of the HOMO-LUMO molecular orbitals allowed us to establish the viability of the studied materials for application in optoelectronic areas. Although we observed notable changes in analogs in the HOMO-LUMO levels in the metallated species, all the elements establish their molecular orbital levels above the conduction band of some anodes such as TiO₂ and ZnO₂ and below some redox couples used for the regeneration of the sensitizer in solar cells. Furthermore, these compounds present such expansive windows between the oxidation and reduction peaks that they could allow generating sensitive layers for the development of electrochemical sensors in detecting analytes of interest or based on their metal centers, generate compounds that can be used in areas such as electrocatalysis.

Acknowledgements

We gratefully acknowledge Consejo Nacional de Ciencia y Tecnología (CONACyT, GRANT No. 242823) and the graduate scholarship (No. 632786) for supporting this project. We also acknowledge Tecnológico Nacional de México for supporting this project (No. 7814-20P).

References

1. Weerth, R. S.; Dailey Harry A., J.; Medlock, A. E. Elsevier: Oxford, **2021**. 386-394. DOI: <https://doi.org/10.1016/B978-0-12-819460-7.00075-X>.
2. Yang, F.; Xu, M.; Chen, X.; Luo, Y.; *Biomed. Pharmacother.* **2023**, *164*, 114933. DOI: <https://doi.org/10.1016/j.biopha.2023.114933>.
3. Pandey, V.; Jain, D.; Pareek, N.; Gupta, I. *Inorganica Chim. Acta.* **2020**, *502*, 119339. DOI: <https://doi.org/10.1016/j.ica.2019.119339>.
4. Martins, M. B. M. S.; Corrêa, G. A.; Moniz, T.; Medforth, C. J.; de Castro, B.; Rebelo, S. L. H.; *J. Catal.* **2023**, *419*, 125-136. DOI: <https://doi.org/10.1016/j.jcat.2023.02.001>.
5. Pucelik, B.; Sulek, A.; Drozd, A.; Stochel, G.; Pereira, M. M.; Pinto, S. M. A.; Arnaut, L. G.; Dąbrowski, J. M. *Int. J. Mol. Sci.* **2020**, *21*, DOI: <https://doi.org/10.3390/ijms21082786>.
6. Wang, X.; Lv, H.; Sun, Y.; Zu, G.; Zhang, X.; Song, Y.; Zhao, F.; Wang, J. *Spectrochim. Acta Part A Mol. Biomol. Spectrosc.* **2022**, *279*, 121447. DOI: <https://doi.org/10.1016/j.saa.2022.121447>.
7. Zhang, X.; Wang, J.; Juan, Y.; Yang, H.; Wei, W.; Zhao, J. *Spectrochim. Acta Part A Mol. Biomol. Spectrosc.* **2022**, *274*, 121136. DOI: <https://doi.org/10.1016/j.saa.2022.121136>.
8. Tang, F.; Wu, J.; Lin, Z.; Wu, H.; Peng, X. *Appl. Surf. Sci.* **2023**, *635*, 157720-. DOI: <https://doi.org/10.1016/j.apsusc.2023.157720>.
9. Paul-Roth, C. O.; Simonneaux, G. *Comptes Rendus Chim.* **2006**, *9*, 1277-1286. DOI: <https://doi.org/10.1016/j.crci.2006.04.003>.
10. Nascimento, B. F. O.; Pineiro, M.; Rocha Gonsalves, A. M. d'A.; Ramos Silva, M.; Matos Beja, A.; Paixão, J. A. *J. Porphyr. Phthalocyanines.* **2007**, *11*, 77-84. DOI: <https://doi.org/10.1142/S1088424607000102>.
11. Yaseen, M.; Ali, M.; NajeebUllah, M.; Ali Munawar, M.; Khokhar, I. *J. Heterocycl. Chem.* **2009**, *46*, 251-255. DOI: <https://doi.org/10.1002/jhet.78>.
12. Boscencu, R. *Molecules.* **2011**, *16*, 5604-5617. DOI: <https://doi.org/10.3390/molecules16075604>.
13. Henriques, C. A.; Pinto, S. M. A.; Pineiro, M.; Canotilho, J.; Eusébio, M. E. S.; Pereira, M. M.; Calvete, M. J. F. *RSC Adv.* **2015**, *5*, 64902-64910. DOI: <https://doi.org/10.1039/C5RA11820D>.
14. Castro-Cruz, H. M.; Macías-Ruvalcaba, N. A. *Coord. Chem. Rev.* **2022**, *458*, 214430. DOI: <https://doi.org/10.1016/j.ccr.2022.214430>.
15. O'Neill, J. S.; Boyle, N. M.; Marques Passos, T.; Heintz, K.; Browne, W. R.; Quilty, B.; Pryce, M. T. *J. Photochem. Photobiol. A Chem.* **2023**, *438*, 114573. DOI: <https://doi.org/10.1016/j.jphotochem.2023.114573>.
16. Zhang, J.; Zhang, Y.; Cao, T.; Zhou, Y.; Dong, L.; Liu, L.; Tong, Z. *Mater. Chem. Phys.* **2023**, *307*, 128225. DOI: <https://doi.org/10.1016/j.matchemphys.2023.128225>.
17. Zhao, J.; Lyu, H.; Wang, Z.; Ma, C.; Jia, S.; Kong, W.; Shen, B. *Sep. Purif. Technol.* **2023**, *312*, 123404. DOI: <https://doi.org/10.1016/j.seppur.2023.123404>.
18. Karthikeyan, S.; Lee, J. Y. *J. Phys. Chem. A*, **2013**, *117*, 10973-10979. DOI: <https://doi.org/10.1021/jp408473k>.

19. Adler, A. D.; Longo, F. R.; Finarelli, J. D.; Goldmacher, J.; Assour, J.; Korsakoff, L. *J. Org. Chem.* **1967**, 32, 476. DOI: <https://doi.org/10.1021/jo01288a053>.
20. Önal, E.; Ay, Z.; Yel, Z.; Ertekin, K.; Gürek, A. G.; Topal, S. Z.; Hirel, C. *RSC Adv.* **2016**, 6, 9967-9977. DOI: <https://doi.org/10.1039/C5RA24817E>.
21. Lindsey, J. S.; Schreiman, I. C.; Hsu, H. C.; Kearney, P. C.; Marguerettaz, A. M. *J. Org. Chem.* **1987**, 52, 827-836. DOI: <https://doi.org/10.1021/jo00381a022>.
22. León-Cedeño, F.; Menes-Arzate, M.; García-Ortega, H. *Rev. Cuba. Química.* **2006**, XVIII, 140-143. DOI: <https://www.redalyc.org/articulo.oa?id=443543704044>.
23. Bandgar, B. P.; Gujarathi, P. B. *J. Chem. Sci.* **2008**, 120, 259-266. DOI: <https://doi.org/10.1007/s12039-008-0031-2>.
24. Queirós, C.; Leite, A.; Moura, N. M. M.; Cerqueira, A. F. R.; Serra, V. V.; Neves, M. G. P. M. S.; Tomé, A. C.; Silva, A. M. G. *Dye. Pigment.* **2023**, 217, 111431. DOI: <https://doi.org/10.1016/j.dyepig.2023.111431>.
25. Taniguchi, M.; Lindsey, J. S.; Bocian, D. F.; Holten, D. *J. Photochem. Photobiol. C Photochem. Rev.* **2021**, 46, 100401. DOI: <https://doi.org/10.1016/j.jphotochemrev.2020.100401>.
26. Liang, Z.; Guo, H.; Lei, H.; Cao, R. *Chinese Chem. Lett.* **2022**, 33, 3999-4002. DOI: <https://doi.org/10.1016/j.cclet.2021.11.055>.
27. Mušković, M.; Džeba, I.; Antol, I.; Basarić, N.; Malatesti, N. *J. Photochem. Photobiol. A Chem.* **2023**, 444, 114939. DOI: <https://doi.org/10.1016/j.jphotochem.2023.114939>.
28. Ghosh, A.; Steene, E. *J. Biol. Inorg. Chem.* **2001**, 6, 739-752. DOI: <https://doi.org/10.1007/s007750100275>.
29. Tangen, E.; Ghosh, A. *J. Am. Chem. Soc.* **2002**, 124, 8117-8121. DOI: <https://doi.org/10.1021/ja0126935>.
30. Roy, D. R.; Shah, E. V.; Mondal Roy, S. *Spectrochim. Acta Part A Mol. Biomol. Spectrosc.* **2018**, 190, 121-128. DOI: <https://doi.org/10.1016/j.saa.2017.08.069>.
31. Haas, M.; Krisch, D.; Gonglach, S.; Bechmann, M.; Scharber, M. C.; Ertl, M.; Monkowius, U.; Schöfberger, W. *European J. Org. Chem.* **2021**, 10, 1525-1537. DOI: <https://doi.org/10.1002/ejoc.202100097>.
32. Alkorta, I.; Elguero, J.; Silva, A. M. S.; Tomé, A. C. *J. Porphyr. Phthalocyanines*, **2010**, 14, 630-638. DOI: <https://doi.org/10.1142/S1088424610002409>.
33. Granados-Oliveros, G.; Ortega, F. M.; Páez-Mozo, E.; Ferronato, C.; Chovelon, J. M. *Open Mater. Sci. J.* **2010**, 4, 15-22. DOI: <https://doi.org/10.2174/1874088X01004020015>.
34. Gouterman, M.; Wagnière, G. H.; Snyder, L. C. *J. Mol. Spectrosc.* **1963**, 11, 108-127. DOI: [https://doi.org/10.1016/0022-2852\(63\)90011-0](https://doi.org/10.1016/0022-2852(63)90011-0).
35. Donohoe, C.; Charisiadis, A.; Maguire, S.; Twamley, B.; Schaberle, F. A.; Gomes-da-Silva, L. C.; Senge, M. O. *European J. Org. Chem.* **2023**, 26, 8-19. DOI: <https://doi.org/10.1002/ejoc.202201453>.
36. Laba, K.; Lapkowski, M.; Officer, D. L.; Wagner, P.; Data, P. *Electrochim. Acta.* **2020**, 330, 135140. DOI: <https://doi.org/10.1016/j.electacta.2019.135140>.
37. Castro-Riquelme, C. L.; Ochoa-Terán, A.; Calva-Yáñez, J. C.; Reynoso-Soto, E. A.; Félix-Navarro, R. M. *Mater. Renew. Sustain. Energy.* **2021**, 10, 2. DOI: <https://doi.org/10.1007/s40243-021-00190-0>.
38. Cardona, C. M.; Li, W.; Kaifer, A. E.; Stockdale, D.; Bazan, G. C. *Adv. Mater.* **2011**, 23, 2367-2371. DOI: <https://doi.org/10.1002/adma.201004554>.
39. Altmann, A.; Eden, M.; Hüttmann, G.; Schell, C.; Rahmzadeh, R. *Food Packag. Shelf Life.* **2023**, 38, 101105. DOI: <https://doi.org/10.1016/j.fpsl.2023.101105>.
40. Balu, K.; Kaliyamoorthy, S.; Durai, M.; Aguiar, A.; Sobral, M. C. M.; Muthuvel, I.; Kumaravel, S.; Avula, B.; Sobral, A. J. F. N.; Ahn, Y.-H. *Inorg. Chem. Commun.* **2023**, 154, 110973. DOI: <https://doi.org/10.1016/j.inoche.2023.110973>.

41. Abu Talip, R. A.; Yahya, W. Z. N.; Bustam, M. A. *J. Mol. Liq.* **2022**, 346, 118270. DOI: <https://doi.org/10.1016/j.molliq.2021.118270>.
42. Li, X.; Su, Y.; Ma, Y.; Wei, L.; He, Y.; Gu, Y.; Mei, S.; Mu, Q.; Peng, C.; Peng, Y.; Deng, Z. *Appl. Catal. B Environ.* **2023**, 337, 122964. DOI: <https://doi.org/10.1016/j.apcatb.2023.122964>.
43. Iordache, A.-M.; Cristescu, R.; Fagadar-Cosma, E.; Popescu, A. C.; Ciucu, A. A.; Iordache, S. M.; Balan, A.; Nichita, C.; Stamatina, I.; Chrisey, D. B. *Comptes Rendus Chim.* **2018**, 21, 270-276. DOI: <https://doi.org/10.1016/j.crci.2017.05.008>.
44. Arceo-Ruiz, H.; Xochitiotzi-Flores, E.; García-Ortega, H.; Farfán, N.; Santillan, R.; Rincón, S.; Zepeda, A. *Molecules.* **2023**, 28, 1816. DOI: <https://doi.org/10.3390/molecules28041816>.